High latitude peaks in Mercury's sodium exosphere: Spectral signature using THEMIS solar telescope

François Leblanc, Alain Doressoundiram, N. Schneider, V. Mangano, A. López Ariste, C. Lemen, B. Gelly, C. Barbieri, Gabriele Cremonese

High latitude peaks in Mercury's sodium exosphere: Spectral signature using THEMIS solar telescope

F. Leblanc,[1] A. Doressoundiram,[2] N. Schneider,[3] V. Mangano,[4] A. López Ariste,[5] C. Lemen,[6] B. Gelly,[5] C. Barbieri,[7] and G. Cremonese[8]

Received 11 July 2008; revised 15 August 2008; accepted 21 August 2008; published 25 September 2008.

[1] We present the first combined intensity and temperature maps of sodium in Mercury's exosphere, made possible by the use of the THEMIS solar telescope on Tenerife in the Canary Islands. The intensity maps clearly show high-latitude peaks, and temperatures inferred from spectral line widths suggest that these regions are either slightly hotter than the rest of the exosphere or much smaller than observed. These brighter, warmer regions are also observed, for the first time, to appear within few Earth hours which strongly suggest that they are produced by solar wind sputtering. This highly capable instrument obtained these data during daylight, highlighting the unique potential for THEMIS to undertake continuous multi-hour and multi-day datasets in conjunction with the MESSENGER mission to Mercury. **Citation:** Leblanc, F., A. Doressoundiram, N. Schneider, V. Mangano, A. López Ariste, C. Lemen, B. Gelly, C. Barbieri, and G. Cremonese (2008), High latitude peaks in Mercury's sodium exosphere: Spectral signature using THEMIS solar telescope, *Geophys. Res. Lett.*, *35*, L18204, doi:10.1029/2008GL035322.

1. Introduction

[2] Twenty years after the discovery of the sodium exospheric emission at Mercury [*Potter and Morgan*, 1985], a large body of observational data has led to a partial understanding of the sources and sinks of Mercury's sodium exosphere. In particular, long term observational programs provided a statistically significant sampling of the annual [*Potter et al.*, 2007] and diurnal cycles [*Sprague et al.*, 1997; *Potter et al.*, 2006]. High latitude bright peaks of sodium emission have been frequently observed [*Potter et al.*, 2006] and shown to be variable on a time scale of the order of the Earth's day. Many ejection mechanisms have been suggested [*Leblanc et al.*, 2007], each one having its own spatial, temporal and energetic signatures. *Potter and Morgan* [1987] used the Coudé echelle spectrograph of the McDonald Observatory with a spectral resolution of 7.6 mÅ and concluded that the spectral signature of the exospheric sodium atoms is in agreement with a population of 500 K, that is, thermalized with the surface, a result later revised by *Shemansky and Morgan* [1991] who concluded that such a spectral signature might be consistent with a 1000 K population. *Killen et al.* [1999] performed slit observations using the Coudé echelle spectrograph of the McDonald Observatory with an improved spectral resolution of 7.2 mÅ as well as using the Anglo Australian Telescope (AAT) with 6.1 mÅ spectral resolution with a $1'' \times 1.5''$ aperture. *Killen et al.* [1999] confirmed *Shemansky and Morgan* [1991] conclusions. In this paper, we describe observations of Mercury's sodium exosphere obtained at the THEMIS Solar Telescope with lower spectral resolution but with imaging capability (section 2) so that high latitude bright emission peaks and spectral signatures could be compared (section 3) and discussed (section 4).

2. Observations and Analysis

[3] THEMIS [*López Ariste et al.*, 2000] is a French-Italian solar telescope on the Canary Island of Tenerife with a 0.9 m primary mirror (with a central obscuration of 0.4 m) and a 15.04 m focal length. The slit size was $0.5'' \times 2'$ and the spectral resolution of 27 mÅ provided ~220,000 resolving power. Two individual cameras are used to simultaneously measure small spectral regions around the D_1 at 5896 Å and D_2 at 5890 Å Na emission lines. Each camera covers a spectral range of ~6 Å and is composed of 512 by 512 pixels at 10.2 mÅ/pixel spectral dispersion. The first observation was obtained on the 1st June 2007 between 15:26 and 17:16 UT (16:26–18:16 local time). Mercury's true anomaly angle (TAA) was 117°, the phase angle was 103° and Mercury's radius (R_M) was 4.02″. Mercury's heliocentric distance was 0.413 AU and its heliocentric velocity was +8.7 km/s (away from the Sun). The second observation was obtained on the 23 April 2008 (TAA = 347°, phase angle = 26°, Mercury heliocentric distance = 0.31 AU and velocity = −2.3 km/s).

[4] Mercury's exosphere was scanned over 16 positions in June 2007 and 21 positions in April 2008 with the slit moved one slit width perpendicular to the slit between each position automatically. The telescope provided tip-tilt corrections at ~1 kiloHertz. At each slit position, twenty individual exposures of twenty seconds were taken for a total length of 6400 s and 8400 s in June 2007 and April 2008 respectively with negligible overhead for CCD read-out and slit motions. The data were bias corrected and flat fielded. The flat field was obtained by observing the Sun using a special mode avoiding solar bright or dark spots. Spectral calibration was carefully performed by identifying telluric lines on a sky spectrum obtained during the same day. The sky background was calculated from two segments

[1]Service d'Aéronomie, Université Versailles Saint Quentin, CNRS, Verrières-Le-Buisson, France.
[2]Observatoire de Paris-Meudon, LESIA, Meudon, France.
[3]LASP, University of Colorado, Boulder, Colorado, USA.
[4]INAF-IFSI, Rome, Italy.
[5]THEMIS, CNRS, UPS853, La Laguna, Spain.
[6]THEMIS, La Laguna, Spain.
[7]Department of Astronomy, University of Padua, Padua, Italy.
[8]Osservatorio Astronomico di Padova, INAF, Padua, Italy.

0094-8276/08/2008GL035322

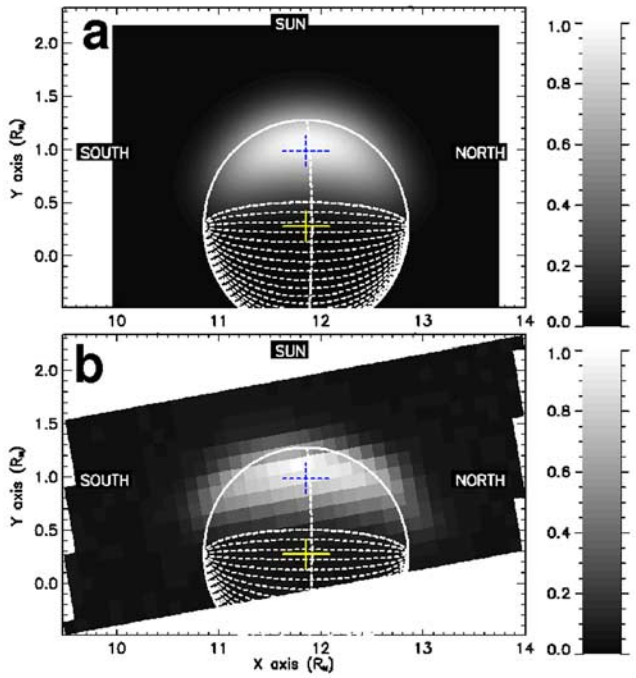

Figure 1. Mercury' surface reflectance normalized to the peak of reflectance (dashed cross). Mercury's disk is indicated, the solid cross corresponds to its center. The white dashed lines are longitudes on the nightside region. (a) Theoretically calculated reflectance. (b) Measured continuum near the D_2 emission line.

of 18″ length at 30″ distance from Mercury's position at each end of the slit. The measured signal was then interpolated over the whole slit by fitting these two parts with a second degree polynomial, and the result of this interpolation was subtracted from the spectra.

[5] In order to subtract the reflected solar spectrum from Mercury's surface, we used the BASS 2000 solar spectrum http://bass2000.obspm.fr) reduced in resolution to match THEMIS. The exospheric emission line is then integrated subtracting an average background level calculated outside the emission line. We also calculated the center of the exospheric emission line and estimated its Doppler shift with respect to Mercury. At the end, we fitted the emission line with a Gaussian function and derived the spectral full width at half maximum (FWHM) of the emission line after correction by the effect of the point spread function of the telescope.

[6] The calibration in brightness is based on the Hapke theoretical model of the reflected solar light from Mercury's surface [*Mallama et al.*, 2002] which has the advantage of avoiding any uncertainty due to Earth's atmospheric absorption [*Sprague et al.*, 1997]. The continuum measured along the slit is calculated outside the Fraunhofer solar absorption line and away from telluric lines. We calculated the centroid of the pixels where the continuum is above 50% of the maximum measured continuum and a theoretical Mercury disk for the illumination geometry, blurred by an initial guess for the atmospheric seeing. The theoretical Mercury disk is then placed in the frame of the observation by aligning its centroid of reflected light with the centroid of the data. In order to evaluate the impact of the uncertainty on Mercury's position on the seeing estimate, we then considered twenty positions of Mercury's disk distributed perpendicularly to the slit within ±0.2″ from this first position. For each position and for each slit with good signal/noise (S/N) ratio of the continuum, we then recalculated the seeing value which provided the best fit by Hapke theoretical reflectance profile of the measured continuum along these slits. The set of seeing values calculated by this method provided the most probable seeing value and its standard deviation. Figure 1 provides the comparison between theoretical reflectivity of Mercury's disk and observed D_2 continuum in June 2007 giving a FWHM seeing of 2.06″ ± 0.37″ (and 2.13″ ± 0.38″ when using the D_1 continuum) The theoretical peak of reflectivity as well as the standard deviation on this value (derived from the standard deviation on the seeing value) is then compared to the maximum value of the measured continuum, providing a calibration factor.

3. Results

[7] Figure 2 shows two localized peaks in brightness on both D_1 and D_2 lines apparent at high northern and southern latitudes (June 2007). *Potter et al.* [2006] highlighted the occurrence of such symmetrical high latitude peaks in correlation with large solar radiation pressure, as is the case here. At TAA = 117°, a summed D_2 emission brightness between 1.0 and 1.7 10^5 kilo-Rayleigh (kR) has been reported by *Potter et al.* [2007]. The Rayleigh unit is a measure of the omnidirectional emission rate in a column of unit cross section along the line of sight, with 1 R = 10^6 photon/cm^2/s [*Chamberlain and Hunten*, 1987]. We mea-

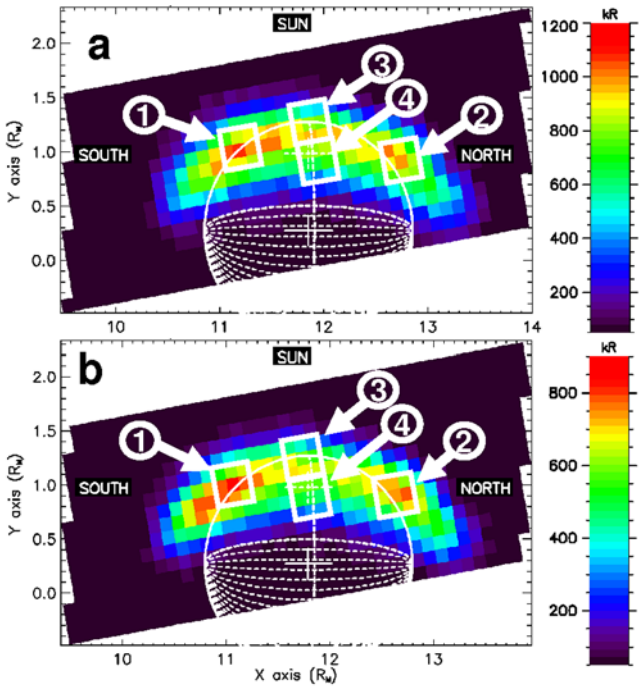

Figure 2. Measured emission brightness. (a) D_2 emission brightness in kR. (b) D_1 emission brightness in kR. The squares labeled 1, 2, 3 and 4 are FWHM comparison zones discussed in the text. The seeing was 0.5 R_M (2.1 ± 0.4″).

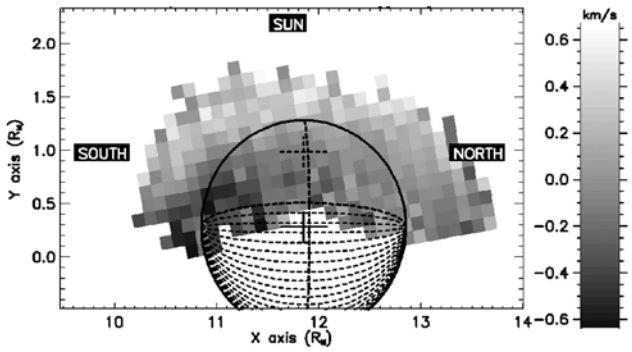

Figure 3. Measured Doppler shift as deduced from the D_2 emission line. We plotted only pixels with S/N larger than 40.

sured a summed D_2 emission brightness equal to 1.19 ± 0.08 10^5 kR in good agreement with *Potter et al.* [2007].

[8] Figure 3 displays the measured Doppler shift (June 2007) with respect to the observer in Mercury's frame as inferred from the D_2 emission line (mean Doppler shift 0.02 km/s). The Doppler shift derived from the D_1 line displays the same trend with a decrease of the shift in the anti-sunward direction. We note a global −0.6 km/s difference in shift with respect to the D_2 line, a difference which is larger than the 0.3 km/s uncertainty due to the spectral dispersion. We attribute this difference between D_1 and D_2 Doppler shift to the uncertainty induced by the subtraction of the continuum and sky. The anti-sunward decrease of the Doppler shift may be due to the radiation pressure or to the phase angle. Indeed, the particles, if preferentially ejected along a direction normal to the surface, would be ejected away from the observer (positive Doppler shift) for positions close to the limb and at the terminator towards the observer (negative shift) at the terminator as observed.

[9] Figure 4 displays the result of the calculated spectral width (FWHM) of both D_2 and D_1 exospheric emission lines in June 2007. Only FWHM values in a pixel with large S/N ratio and with value of the derived FWHM larger than the spectral resolution (1.4 km/s) are displayed in Figure 4. Contrary to the Doppler shift, the method used to subtract sky and continuum does not impact significantly the calculated spectral width.

[10] There is a spatial coincidence between the positions of the peak brightness (Figure 2) and regions of large spectral width (Figure 4). If we define squared zones centred on the two peaks of emission (as shown in Figures 2 and 4 by the squares 1 and 2) and along Mercury's equator (squares 3 and 4), the FWHM of the average spectrum measured within these pixels is equal to 2.76, 2.74, 2.66 and 2.54 km/s within squares 2, 1, 3 and 4 respectively (D_2 line). The uncertainty induced by the noise on the calculated spectral width can be derived supposing that the spectrum is a Gaussian function $F(x) = A \times \exp(-x^2/\sigma^2)$. An error r on the measured signal F will imply an error δ on x as $F(x) + r = F(x+\delta)$ which can be solved considering the value of $x = \sigma\sqrt{\ln 2}$ at the FWHM of F: $\delta = -\sigma\sqrt{\ln 2} \times \left(1 \pm \sqrt{1 - \ln\left(2\frac{r}{A} + 1\right)/\ln 2}\right)$. In this equation, the term in bracket represents half the uncertainty on the FWHM and is expressed in term of the noise/signal ratio r/A which is equal to ∼0.025, so that the fractional uncertainty on the FWHM is ∼0.07 or 0.2 km/s at 2.75 km/s, therefore of the order of the difference between the observed FWHM. We performed an analysis of the statistical meaning to find large value of FWHM within predefined areas. Starting from the FWHM distribution as measured within all pixels displayed in Figure 4, we have randomly distributed these values within a 2D map of the same size (∼12 × 30 pixels) and have counted the number of time the two predefined areas of pixels had simultaneously spectral width larger than 2.75 km/s and 2.73 km/s. We found a probability of less than 1.5 % for the D_2 line. We also measured FWHM values of the D_1 line equal to 2.74, 2.69, 2.53 and 2.66 km/s (squares 2, 1, 3 and 4 respectively) and found a probability of 44%. Therefore, the probability to find both D_1 and D_2 FWHM peaks in correlation with both D_1 and D_2 peaks of emission is less than 0.7 %.

[11] Figure 5 is another example of THEMIS observation obtained on the 23 April 2008. The signal is fainter than on the 06/01/07 because Mercury was close to its perihelion and therefore at a low Doppler shift. In Figure 5, there is a clear peak appearing in the southern hemisphere as illustrated by Figure 5b when compared to Figure 5a. Such a peak is associated to a clear increase of the spectral width as shown in panel d with respect to the spectral width map which was measured one hour before (Figure 5c). We exclude that the change in distribution from Figures 5a to 5b may be due to seeing effect since both associated continuum images display very similar shape. This is the first time that such a local variation of Mercury's exosphere on Earth's hour time scale is reported.

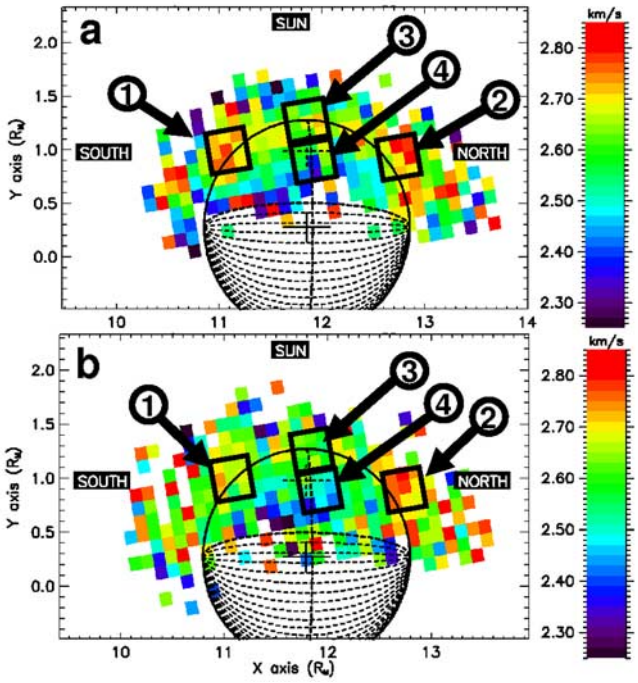

Figure 4. Measured spectral width. (a) As deduced from the D_2 emission line. (b) As deduced from the D_1 emission line. We plotted only pixels with S/N larger than 40.

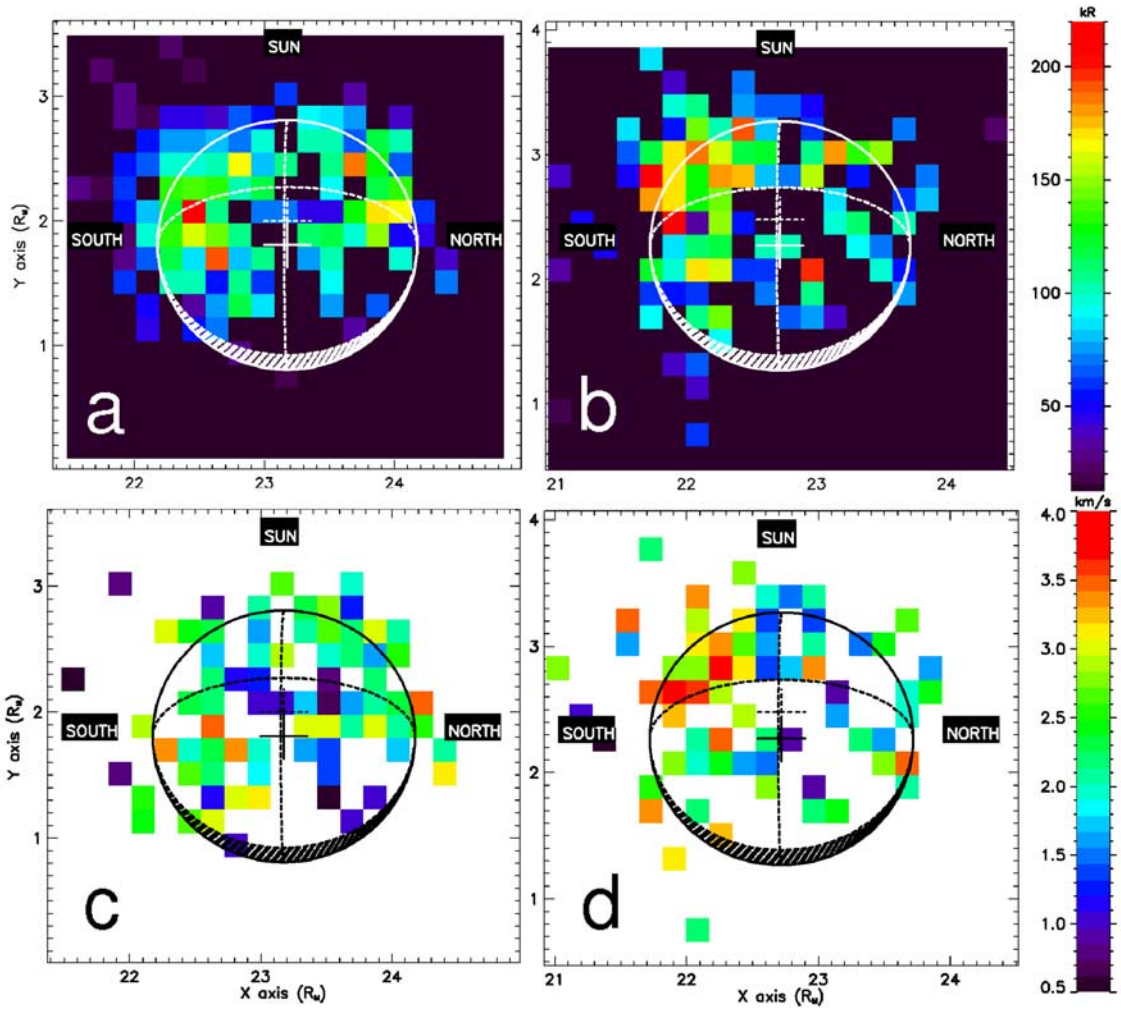

Figure 5. April 23, 2008, THEMIS observation. The seeing was 0.4 RM: (a, c) $1.9 \pm 0.4''$ and (b, d) $2.1 \pm 0.4''$. Panels a and b: Measured D_2 emission brightness (kR). Panels c and d: spectral width of the D_2 emission line. For Figures 5a and 5c: scan done between 9:13 and 11:36 UT. For Figures 5b and 5d: scan done between 11:42 and 12h54 UT.

[12] The correlation between intensity and FWHM could have three possible causes: (1) instrumental/analysis artifacts; (2) line broadening due to optical depth effects; (3) different ejection processes from Mercury's surface. We disproved the first possibility, that the analysis finds greater FWHM for brighter lines, by adding comparison spectrum emissions of different brightnesses into the Mercury spectra. We found no correlation between brightness and derived line width. We are therefore left with two explanations for this correlation. The curve of growth of D_1 versus D_2 line intensities is linear for the full range of observed intensities, which suggests an optically thin Na exosphere. The D_2 emission brightness peaks at ~1200 kR, which following the *Brown and Yung* [1976] formulation of the relation between emission brightness and column density extrapolated to Mercury corresponds to column density of $N \sim 5 \times 10^{10}$ Na/cm^2. Following their methodology, we find for T = 1000 K $\tau_{D2} = 0.3$, $\tau_{D1} = 0.15$ and $\tau_{D2} = 0.2$, $\tau_{D1} = 0.1$ for T = 2000 K. Therefore, the peaks of emission brightness are optically thin or only slightly thick if the spatial size of the emission peaks is not significantly smaller than observed. If that case, we are left with the final possibility, that the brighter emissions are broader due to higher velocities perhaps attributed to more energetic ejection in the high-latitude spots. In the optically thin limit, it is possible to directly derive a kinetic temperature for the exospheric particles along the line of sight by fitting the spectra with a function summed of Gaussian line profiles for all hyperfine levels [*Brown and Yung*, 1976] convolved with the point spread function of the instrument. For D_1+D_2 emission lines obtained within squares 2 and 1, we found temperatures of 927 ± 41 K and within squares 3 and 4 temperatures of 855 ± 60 K. These values are more than 200 K smaller than calculated by *Killen et al.* [1999] which might be due to optical thickness effect (taken into account by *Killen et al.* [1999]) or to differences in Mercury's exosphere.

4. Conclusion

[13] The simultaneous intensity and temperature maps allowed us to extract some original clues on the energetic characteristics of Mercury's sodium exosphere and in par-

ticular on the energetic characteristics of high latitude peaks in emission brightness. Our 2D map of the spectral width of the emission line demonstrates a significant correlation between peaks in brightness and peaks in spectral width. The observed range of spectral widths suggests a globally hotter exosphere than it would be if thermalized with the surface [*Killen et al.*, 1999], the peak of emission being optically thin. However, if the real spatial dimension of this peak is much smaller than the size suggested by our observation, the optical thickness might be much larger so that we cannot rule out definitively a local increase in Doppler width due to a local increase of the optical thickness. If not, this observation suggests that the observed peaks of emission brightness at high latitude have been produced by an ejection mechanism significantly more energetic than the mechanism(s) producing the bulk of the exosphere. This rules out thermal desorption because this process is known as the lesser energetic mechanism. Meteoritic vaporization may produce such energetic signature but it is highly improbable that it might produce two simultaneous high latitude peaks. It could be photo stimulated desorption (PSD) or sputtering. PSD may generate such features only if local maxima of sodium surface density are present at high latitudes [*Leblanc et al.*, 2007]. A strong radiation pressure effect has also been suggested to induce polar limb brightening leading to symmetric peaks in both northern and southern hemispheres [*Potter et al.*, 2006]. But the rapid variation of the exosphere observed in April 2008 is a strong argument for solar wind sputtering which is therefore the most likely explanation for the broader lines in the high latitude spots.

References

Brown, R. A., and Y. L. Yung (1976), *Io, its atmosphere and optical emissions, in Jupiter*, edited by T. Gehrels, 1102 pp., Univ. of Ariz. Press, Tucson.

Chamberlain, J. W., and D. M. Hunten (1987), *Theory of Planetary Atmospheres*, Academic Press, New York.

Killen, R. M., A. E. Potter, A. Fitzsimmons, and T. H. Morgan (1999), Sodium D_2 line profiles: Clues to the temperature structure of Mercury's exosphere, *Planet. Space Sci.*, *47*, 1449.

Leblanc, F., et al. (2007), Mercury's exosphere: Origins and relations to its magnetosphere and surface, *Planet. Space Sci.*, *55*, 1069.

López Ariste, A., J. Rayrole, and M. Semel (2000), First results from THEMIS spectropolarimetric mode, *Astron. Astrophys.*, *142*, 137.

Mallama, A., D. Wang, and R. A. Howard (2002), Photometry of Mercury from SOHO/LASCO and Earth, The Phase Function from 2 to 170, *Icarus*, *155*, 253.

Potter, A. E., and T. H. Morgan (1985), Discovery of sodium in the atmosphere of Mercury, *Science*, *229*, 651.

Potter, A. E., and T. H. Morgan (1987), Variation of sodium on Mercury with solar radiation pressure, *Icarus*, *71*, 472.

Potter, A. E., R. M. Killen, and M. Sarantos (2006), Spatial distribution of sodium on Mercury, *Icarus*, *181*, 1.

Potter, A. E., R. M. Killen, and T. H. Morgan (2007), Solar radiation acceleration effects on Mercury sodium, *Icarus*, *186*, 571.

Shemansky, D. E., and T. H. Morgan (1991), Source processes for the alkali metals in the atmosphere of Mercury, *Geophys. Res. Lett.*, *18*, 1659.

Sprague, A. L., R. W. H. Kozlowski, D. M. Hunten, N. M. Schneider, D. L. Domingue, W. K. Wells, W. Schmitt, and U. Fink (1997), Distribution and abundance of sodium in Mercury's atmosphere, 1985–1988, *Icarus*, *129*, 506.

C. Barbieri, Department of Astronomy, University of Padova, vicolo Osservatorio 2, I-35122 Padova, Italy. (cesare.barbieri@unipd.it)

G. Cremonese, INAF-Osservatorio Astronomico di Padova, vicolo Osservatorio 2, I-35122 Padova, Italy. (cremonese@pd.astro.it)

A. Doressoundiram, Observatoire de Paris-Meudon, LESIA, 5 place Jules Janssen, F-92195 Meudon, France. (alain.doressoundiram@obspm.fr)

B. Gelly, C. Lemen, and A. López Ariste, THEMIS, CNRS, UPS, 853 C/ Via Lactea, E-38200 La Laguna, Spain. (bgelly@themis.iac.es; lemen@themis.iac.es; alopez@themis.iac.es)

F. Leblanc, Service d'Aéronomie, Université Versailles Saint Quentin, CNRS, Réduit de Verrières, F-91371 Verrières Le Buisson, France. (francois.leblanc@aerov.jussieu.fr)

V. Mangano, INAF-IFSI, Via del Fosso del Cavaliere, I-00133 Rome, Italy. (Valeria.Mangano@ifsi-roma.inaf.it)

N. Schneider, LASP, University of Colorado, Campus Box 391, Boulder, CO 80309-0391, USA. (nick.schneider@lasp.colorado.edu)